Title

Using semi-quantitative dynamic contrast-enhanced magnetic resonance imaging parameters to evaluate tumor hypoxia: a preclinical feasibility study in a maxillofacial VX2 rabbit model.

Journal

American Journal of Translational Research, 7(3)

ISSN

1943-8141

Authors

Zheng, Linfeng
Li, Yujie
Geng, Feng
et al.

Publication Date

2015

Am J Transl Res 2015;7(3):535-547
www.ajtr.org /ISSN:1943-8141/AJTR0004712

Original Article

Using semi-quantitative dynamic contrast-enhanced magnetic resonance imaging parameters to evaluate tumor hypoxia: a preclinical feasibility study in a maxillofacial VX2 rabbit model

Linfeng Zheng[1,4*], Yujie Li[1,2*], Feng Geng[3], Sujuan Zheng[5], Ruiling Yan[6], Yuedong Han[7], Qiben Wang[8], Zhuoli Zhang[4], Guixiang Zhang[1]

[1]Department of Radiology, Shanghai First People's Hospital, Shanghai Jiao Tong University, Shanghai 200080, China; [2]Department of Radiology, Zhangjiagang First People's Hospital, Zhangjiagang 215600, China; [3]Division of The Thyroid Gland and Breast Surgery, Department of Surgery, Zhangjiagang First People's Hospital, Zhangjiagang 215600, China; [4]Department of Radiology, Feinberg School of Medicine, Northwestern University, Chicago, IL 60611, USA; [5]Dengfeng People's Hospital, Zhengzhou 452470, China; [6]Department of Ultrasound, General Hospital of Lanzhou Military Region, Lanzhou 730050, China; [7]Department of Radiology, General Hospital of Lanzhou Military Region, Lanzhou 730050, China; [8]Department of Histology and Embryology, Xiangya School of Medicine, Central South University, Changsha 410013, China. [*]Equal contributors.

Received December 10, 2014; Accepted February 8, 2015; Epub March 15, 2015; Published March 30, 2015

Abstract: Purpose: To test the feasibility of semi-quantitative dynamic contrast-enhanced magnetic resonance imaging (DCE-MRI) parameters for evaluating tumor hypoxia in a maxillofacial VX2 rabbit model. Methods: Eight New Zealand rabbits were inoculated with VX2 cell solution to establish a maxillofacial VX2 rabbit model. DCE-MRI were carried out using a 1.5 Tesla scanner. Semi-quantitative DCE-MRI parameters, maximal enhancement ratio (MER) and slope of enhancement (SLE), were calculated and analyzed. The tumor samples from rabbits underwent hematoxylin-eosin (HE), pimonidazole (PIMO) and vascular endothelial growth factor (VEGF) immunohistochemistry (IHC) staining, and the PIMO area fraction and VEGF IHC score were calculated. Spearman's rank correlation analysis was used for statistical analysis. Results: The MER values of eight VX2 tumors ranged from 1.132 to 1.773 (1.406 ± 0.258) and these values were negatively correlated with the corresponding PIMO area fraction ($p = 0.0000002$), but there was no significant correlation with the matched VEGF IHC score ($p = 0.578$). The SLE values of the eight VX2 tumors ranged from 0.0198 to 0.0532 s^{-1} (0.030 ± 0.011 s^{-1}). Correlation analysis showed that there was a positive correlation between SLE and the corresponding VEGF IHC score ($p = 0.0149$). However, no correlation was found between SLE and the matched PIMO area fraction ($p = 0.662$). The VEGF positive staining distribution predominantly overlapped with the PIMO adducts area, except for the area adjacent to the tumor blood vessel. Conclusions: The semi-quantitative parameters of DCE-MRI, MER and SLE allowed for reliable measurements of the tumor hypoxia, and could be used to noninvasively evaluate hypoxia during tumor treatment.

Keywords: Dynamic contrast-enhanced magnetic resonance imaging (DCE-MRI), hypoxia, semi-quantitative analysis, imaging biomarker, VX2 tumor, rabbits

Introduction

Tumor hypoxia is closely associated with tumor growth, proliferation, metastasis and therapy [1-3]. Studies have shown that most solid tumors contain three components with heterogeneous oxygen metabolism, resulting in different pathophysiologic characteristics in these three different areas (proliferative, quiescent and necrotic areas) [1, 4, 5]. One of these pathophysiologic features of tumor, hypoxia, is common in many tumors and is closely related to the tumor response to conventional therapy, including radiotherapy and chemotherapeutic agents, and its progression and prognosis [2, 5, 6]. Therefore, the development of methods for detecting tumor hypoxia *in vivo* is important to guiding tumor therapy.

Currently, there are invasive and noninvasive modalities, including oxygen electrode measurements and positron emission tomography

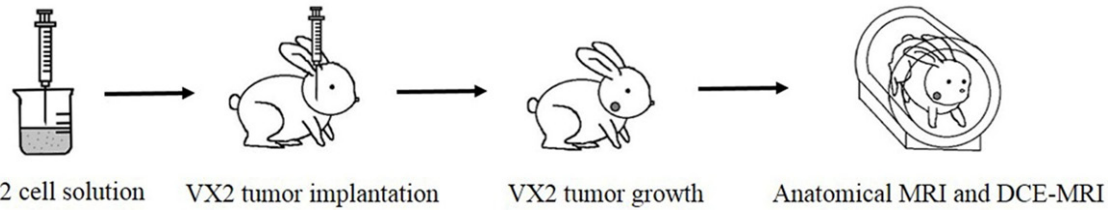

Figure 1. A graphical interpretation of the study design.

(PET), for detecting hypoxia *in vivo* [3, 7]. Oxygen electrode techniques, which directly measure the oxygen levels in tumor, have been successfully applied to many preclinical and clinical studies for assessing the oxygenation of malignancies. Yet, there are some concerns, such as the invasive nature, difficulty of accessing tumors, inability to monitor the entire tumor, inaccuracy in estimating and reading the measurements, capillary and tissue parenchyma damage by electrodes, etc., that have limited its potential usefulness in oncology fields [3, 7, 8]. In recent decades, PET, as a promising non-invasive imaging modality, has emerged for detecting tumor oxygenation *in vivo*. Numerous reports have been published about the application of PET to evaluate hypoxia in tumor biology and therapeutics studies. However, this modality's inherent limitations, including low spatial resolution, inaccuracy of anatomy, the administration of an exogenous radioactive 'tracer', high cost, etc., have hindered it from being an optimal modality for detecting hypoxia in oncology [3, 8, 9]. Clearly, these modalities are not the ideal imaging methods for monitoring tumor hypoxia due to their noted disadvantages. Therefore, the development of a reliable imaging modality or imaging biomarker for measuring the oxygen concentration in tumors is highly warranted.

At present, magnetic resonance imaging (MRI) is increasingly used due to its prominent advantages, such as the lack of radiation, superior soft tissue contrast and availability for anatomical and functional imaging in the oncology field [10-18]. Studies on a variety of animal models and human tumors have shown that MRI can be used for tumor diagnosis and staging, characterization risk stratification, predicting and monitoring the response to treatment, prognosis and follow-up, and the development of new drugs and therapeutic paradigms [10-18]. In particular, dynamic contrast-enhanced magnetic resonance imaging (DCE-MRI) provides morphological and volumetric parameters of the tumors and functional parameters such as contrast enhancement kinetics and perturbations in the tumor blood supply that are related to the tumor oxygenation levels, cellularity and vascularity, which are crucial for cancer management and treatment [10, 12-14, 16]. Our previous studies also showed that functional DCE-MRI can be used to evaluate brain metastases in a rabbit animal model [12], and it can reliably monitor and evaluate the efficacy of combination gene therapy and radiotherapy on a rabbit maxillofacial VX2 tumor *in vivo* using semi-quantitative parameters such as the maximal enhancement ratio (MER) and slope of enhancement (SLE) [19]. Therefore, we hypothesize that functional DCE-MRI can be used to evaluate tumor hypoxia. The purpose of this study is to test the feasibility of DCE-MRI semi-quantitative parameters for evaluating tumor hypoxia in a maxillofacial VX2 rabbit model.

Materials and methods

Study design

This preclinical proof-of-concept study was undertaken using the rabbit VX2 model to validate the semi-quantitative parameters of DCE-MRI for precisely predicting tumor hypoxia. The study was designed to (i) study the feasibility of establishing a rabbit maxillofacial VX2 rabbit model; (ii) conduct a DCE-MRI study and document the semi-quantitative parameters of DCE-MRI; and (iii) measure pathological changes in tumors associated with semi-quantitative parameters of DCE-MRI (**Figure 1**).

Animals

This study fulfilled the recommendations in the guide for the care and use of laboratory animals by the authority of the People's Republic of China. The protocol was approved prior to study by an institutional ethics committee at

Table 1. MRI technical parameters of T1WI, T2WI and DCE-MRI

	Sequence	Acquisition plane	TR (msec)	TE (msec)	FOV (mm)	Matrix	FA	Slice thickness (mm)	In-plane resolution (mm^2)
T1WI	SE	Sagittal, dorsal	350	15	120 × 120	256 × 160	N/A	3	0.35
T2WI	FSE	Sagittal, dorsal	3000	90	120 × 120	256 × 160	N/A	3	0.35
DCE-MRI	GRE	Dorsal	10	2	120 × 120	256 × 160	20°	3	0.35

Note: T1WI = T1-weighted image, T2WI = T2-weighted image, DCE-MRI = dynamic contrast-enhanced magnetic resonance imaging, SE = Spine echo, FSE = Fast spine echo, GRE = Gradient echo, TR = Repetition time, TE = Echo time, FOV = Field of view, FA = Flip angle, and N/A = Not applicable.

Table 2. Summary of clinical features, MRI findings, DCE-MRI parameters and histopathological results in eight rabbits

Case ID	Clinical features			MRI findings					Histopathological results	
				Conventional MRI			DCE-MRI parameters			
	Tumor growth time (Days)	Tumor size (cm^3)	Lymph node metastasis (Yes or No)/ number (n)	T1WI signal	T2WI signal	T1WI enhancement	MER	SLE (s^{-1})	PIMO area fraction (%)	VEGF IHC score
R1	10	0.8	No/0	Iso	Mild hyper	Homogeneous	1.773	0.0236	21	8
R2	12	1.6	No/0	Iso	Mild hyper	Homogeneous	1.773	0.0249	19	8
R3	14	1.5	Yes/1	Iso	Mild hyper	Homogeneous	1.194	0.0234	32	6
R4	16	1.9	No/0	Iso	Mild hyper	Heterogeneous	1.132	0.0365	28	9
R5	18	2.1	Yes/1	Iso	Iso-to-hyper	Homogeneous	1.386	0.0338	21	8
R6	20	2.2	Yes/2	Iso	Iso-to-hyper	Homogeneous	1.236	0.0269	25	6
R7	22	3.7	No/0	Mixed hypo and iso	Mild hyper, with central hyper	Heterogeneous, with irregular central necrosis	1.223	0.0532	27	9
R8	24	5.4	Yes/1	Mixed hypo and iso	Mild hyper with central hyper	Heterogeneous, with irregular central necrosis	1.527	0.0198	22	6

First People's Hospital, Shanghai Jiao Tong University. Eight healthy adult New Zealand white rabbits (weighing 1.2-1.5 kg, no gender limit; purchased from Shanghai Baomu Experimental Animal Farm, Shanghai, China) were enrolled in the present study. All rabbits were anesthetized with a mixture of No.2 Sumianxin (Veterinary Institute, Quartermaster University of PLA, Changchun, China) and ketamine (Shanghai Zhongxi Pharmaceutical (Group) Co., Ltd., Shanghai, China) (1:2.5 v/v; 0.3 ml/kg, intramuscular injection [IM]). All efforts were made to relieve suffering for every procedure.

VX2 tumor cell solution preparation

The implanted VX2 tumor was originally grown in the right hind limb of two donor rabbits (maintained at our institute). When the VX2 tumor in the donor rabbits grew to approximately 1-2 cm in diameter, the donor rabbits were anesthetized with a combination No.2 Sumianxin and ketamine (IM) and held in the prone position on the operation table; the right hind limb hair was shaved and the skin was disinfected with 70% ethyl alcohol. Then, the donor tumors were removed under aseptic surgery and placed in a sterile container with 0.9% saline. After two washes with 0.9% saline, the cell solution was prepared according to our previously published protocol [12, 19] and diluted with 0.9% saline to a cell concentration of approximately 10^6-10^8 cells/ml for the following inoculation.

Maxillofacial VX2 tumor model establishment

Each rabbit enrolled in this study was anesthetized as mentioned above. After anesthesia, the right side of maxillofacial was shaved with a shaver and disinfected with 70% ethyl alcohol. The 0.5 ml VX2 cell solution was injected into each rabbit's masseter muscle, approaching to the angle of the mandible approximately 1 cm with a 2 ml springe. After the tumor inoculation, each rabbit was subcutaneously injected with meloxican (0.3 mg/kg) every 24 hour for up to four days. The inoculated rabbits were returned to storage facilities with free access to water, regular food and a normal light-dark cycle for tumor growth and subsequent study.

MRI

When the tumors grew to the required volumes after 1-4 weeks of inoculation, the MR studies were undertaken using a 1.5 Tesla clinical Signa Horizon MRI scanner with a knee coil (GE Medical Systems, Waukesha, WI, USA). The rabbits were placed in the prone position and the different sequences' images, including the T1-weighted image (T1WI), T2-weighted image (T2WI) and DCE-MRI image, were acquired under combination No.2 Sumianxin of ketamine anesthesia. The T1WI acquisition parameters were as follows: sagittal and dorsal plane acquisition, spine echo (SE) sequence, field of view (FOV) of 120 mm × 120 mm, matrix of 256 × 160, repetition time (TR)/echo time (TE) of 350/15 msec, slice thickness of 3.0 mm, in-plane resolution of 0.35 mm^2, slice interval of 0.5 mm, number of excitations (NEX) of 2, free-breathing and no trigger (**Table 1**). T2WI was obtained with sagittal and dorsal plane acquisition, fast SE sequence, FOV of 120 mm × 120 mm, matrix of 256 × 160, TR/TE of 3000/90 msec, slice thickness of 3.0 mm, slice interval of 0.5 mm, in-plane resolution of 0.35 mm^2, echo train length of 12-18, NEX of 2, free-breathing and no trigger (**Table 1**). DCE-MRI scans were performed with dorsal plane acquisition, a gradient echo (GRE) sequence, FOV of 120 mm × 120 mm, matrix of 256 × 160, TR/TE of 10/2 msec, slice thickness of 3.0 mm, slice interval of 0.5 mm, in-plane resolution of 0.35 mm^2, flip angle (FA) of 20°, NEX of 1, free-breathing and no trigger (**Table 1**). We first performed T1WI and T2WI acquisition sequentially and then obtained a mapping image prior to DCE-MRI scanning. After these, DCE-MRI was started simultaneously with an intravenous (IV) injection of gadolinium-diethylenetriamine pentaacetic acid (Gd-DTPA; Magnevist, 1 ml/kg, Bayer Schering Pharma AG, Berlin, Germany) and repeated at 12, 18, 42 and 150 sec into the examination (**Figure 2A-C**). IV bolus injection of Gd-DTPA was administered via ear vein using an automatic power injector at a 0.2 ml/sec flow rate. The total acquisition time and DCE-MRI slice was 152 sec, for 60 slices, respectively. Finally, the conventional contrast-enhanced T1WI was carried out with the aforementioned parameters.

Image interpretation and DCE semi-quantitative analysis

Two radiologists (YL and GZ, with 10 and 20 years of MRI experience, respectively) analyzed the image data. First, the tumor image features, including the site, number, size, signal, adjacent changes and lymph node metastases, were recorded and read. Second, the maximal

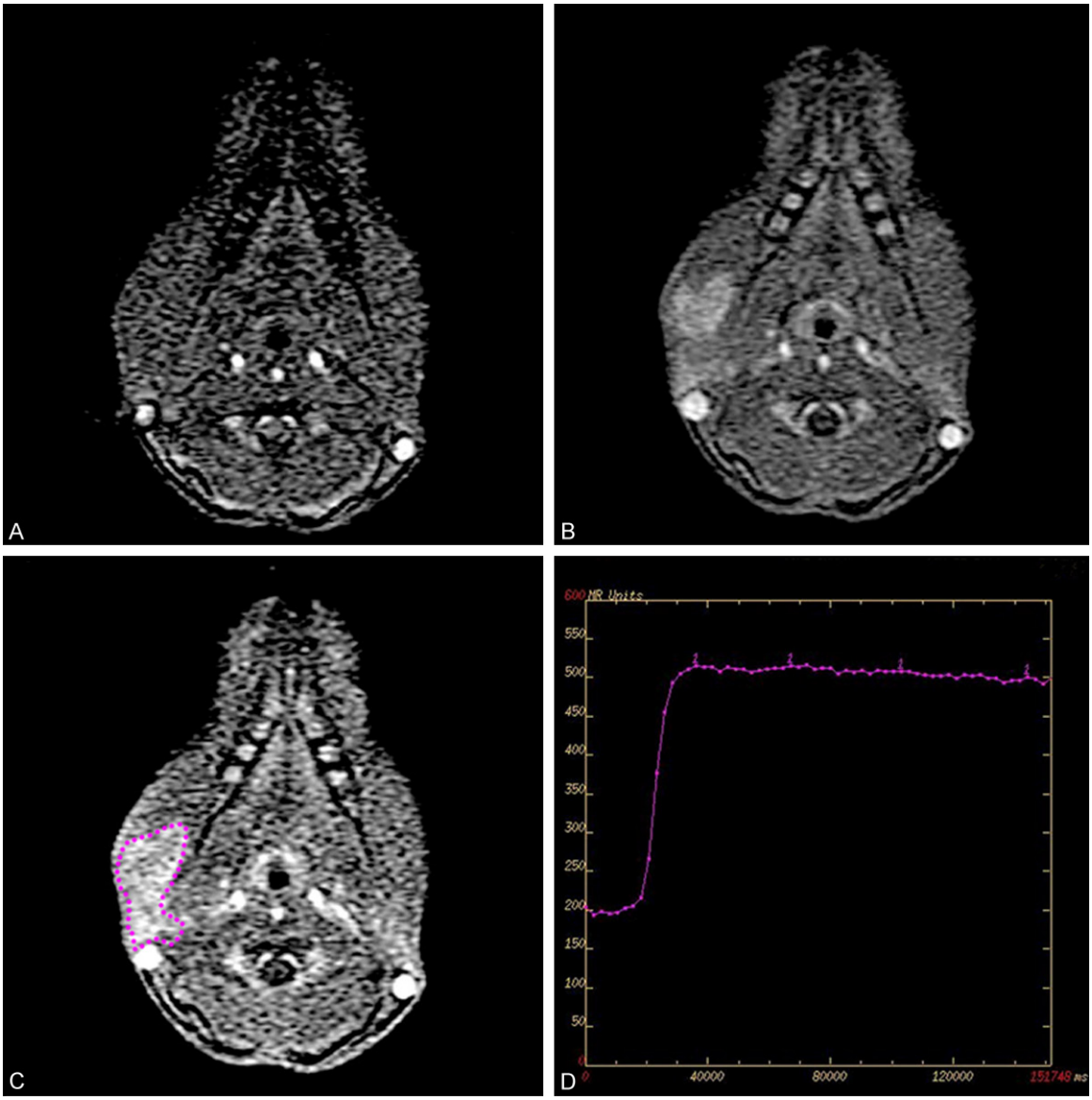

Figure 2. Dynamic contrast-enhanced magnetic resonance imaging (DCE-MRI) and image analysis. Representative DCE-MRI images of tumor at 12 sec (A), 42 sec (B) and 150 sec (C) during DCE-MRI scanning. The dashed line in (C) indicates a representative region of interest (ROI) for image analysis. The time-intensity curve image for image analysis is given in (D).

length (a), width (b), and height (c) of the tumors were measured in a conventional contrast-enhanced T1WI image; then, the tumor volumes (V_{tumor}) were calculated using the formula: V_{tumor} = abc/2 [20]. Finally, we imported the multi-phase DCE-MRI to the image workstation and drew a large region of interest (ROI) approximately covering the entire tumor (**Figure 2C**), except for tumor with distinguishable necrosis. For the latter tumor, a ROI was defined in the tumor area without distinguishable necrosis. The time-signal intensity curve was drawn (**Figure 2D**) for the measurement of the semi-quantitative parameters of DCE-MRI with GE FUNCTOOL software (Advantage workstation version 4.2, GE Medical Systems, Waukesha, WI, USA). The measured parameters were similar to our previous methods [19] and literature [16], which were defined as follows: (a) initial enhancement time (T_{pre}, s), representing when the curve starts to rise; (b) initial enhancement signal (SI_{pre}), representing the relative signal intensity when the curve starts to rise; (c) maximum enhancement time (T_{max}, s), representing

when the curve arrives at a peak; and (d) maximum enhancement signal (SI_{max}), representing the relative signal intensity when the curve arrives at a peak. Finally, the tumor MER was calculated using the formula: MER = (SI_{max} - SI_{pre})/$SI_{pre,}$ and SLE was measured with SLE = MER/(T_{max} - T_{pre}) [19].

Tumor sample preparation

After the MRI scanning, each rabbit was immediately administered 1-[(2-hydroxy-3-piperidinyl)-propyl]-2-nitroimidazole hydrochloride (Pimonidazole hydrochloride, PIMO; Chemicon Int., Temecula, CA, USA) at a dose of 60 mg/kg body weight (freshly dissolved in 0.9% saline) via ear vein for 1 hour. Then, we euthanized the rabbits with sodium pentobarbital (120 mg/kg, intravenous injection) and harvested tumors in each rabbit. Next, the fresh tumors were placed in a container filled with 10% neutral buffered formalin for 24 hours to fix them, which was followed by dehydration with gradient alcohol and embedding with paraffin. Finally, three 5-μm sections were contiguously cut from five sites of each tumor block. For each set of consecutive sections, the first section was stained with hematoxylin-eosin (HE), the second section with PIMO, and the last section with vascular endothelial growth factor (VEGF) immunohistochemistry (IHC). After heating the slides at 40° for 5-6 hours in a warming oven, all were dewaxed with dimethyl benzene (5 min, × 2, at room temperature [RT]) and re-hydrated with gradient alcohol (100%, 100%, 95%, 85%, 70%, 50%, and 30%; each 3 min, × 1; at RT) and distilled water (3 min, × 1, at RT) with the following staining.

HE staining

The standard HE staining was performed according the manufacturer's instructions and our previous method [12, 19].

Detection of tumor hypoxia by PIMO staining

For detection of tumor hypoxia, PIMO staining was performed using HypoxyprobeTM-1 kit (Chemicon Int., Temecula, CA, USA). The intracellular PIMO adducts were detected according to the suggested procedure for immunostaining PIMO adducts in formalin-fixed, paraffin-embedded tissues using a F(ab')2 secondary strategy by the manufacturer and a published method with minor modification [21, 22]. Briefly, the prepared sections were washed with phosphate-buffered saline (PBS, pH = 7.2, 10 mM; 3-5 min, × 3) containing 0.2% BrijTM 35 (Fisher BioReagents, Fair Lawn, NJ, USA); then, the tissue peroxidase was quenched with 3% H_2O_2 (10 min, × 1; at RT), which was followed by PBS washing (3-5 min, × 3). Next, the antigen retrieval of tissues performed with antigen retrieval agents (Chemicon Int., Temecula, CA, USA) at 90° for 20 min and cooled to RT. Then, the non-specific binding site was blocked with 10% fetal bovine serum in a wet incubator box (20 min, at 37°). Next, Hypoxyprobe-1 MAb1 (1:50, 60 min, at 37°), biotin-conjugated F(ab')2 (1:500, 10 min, at RT) and streptavidin peroxidase (10 min, at RT) were consecutively added to the slides and incubated in a wet box. The slides were washed with PBS between every step (3-5 min, × 3). Finally, the slides were incubated with 3,3'-diaminobenzidine (DAB; freshly prepared; Neomarkers, Fermont, CA, USA) chromogen to visualize the antibody complex, and the tumor cells were counterstained with hematoxylin (0.5 min, at RT). All sections were mounted with neutral balsam. For the negative control, the procedure was identical to the aforementioned except for the substitution of Hypoxyprobe-1 MAb1 for PBS.

VEGF IHC staining

Slides consecutive to those stained for PIMO adducts were stained for VEGF with a VEGF IHC kit (Neomarkers, Fermont, CA, USA). The protocol for VEGF IHC staining was used as described in our previous study [19]. VEGF antigen retrieval was carried out using microwave heating (20 min, × 1). The sections were incubated with involved primary VEGF antibody (1:50, 120 min, at 37°), secondary antibody (1:100, 10 min, at RT; Neomarkers, Fermont, CA, USA) and streptavidin peroxidase (10 min, at RT). Other steps were accomplished similarly as noted above for PIMO staining and described previously for the same tumor [19].

Tissue image analysis

All digital images for HE, PIMO and VEGF IHC staining sections were captured using Zeiss Axiovision Image Analysis Software (version 3.1, Carl Zeiss Microscopy, LLC, Thornwood, NY, USA) with a Zeiss Axioplan 2 imaging microscope (Carl Zeiss Microscopy, LLC, Thornwood,

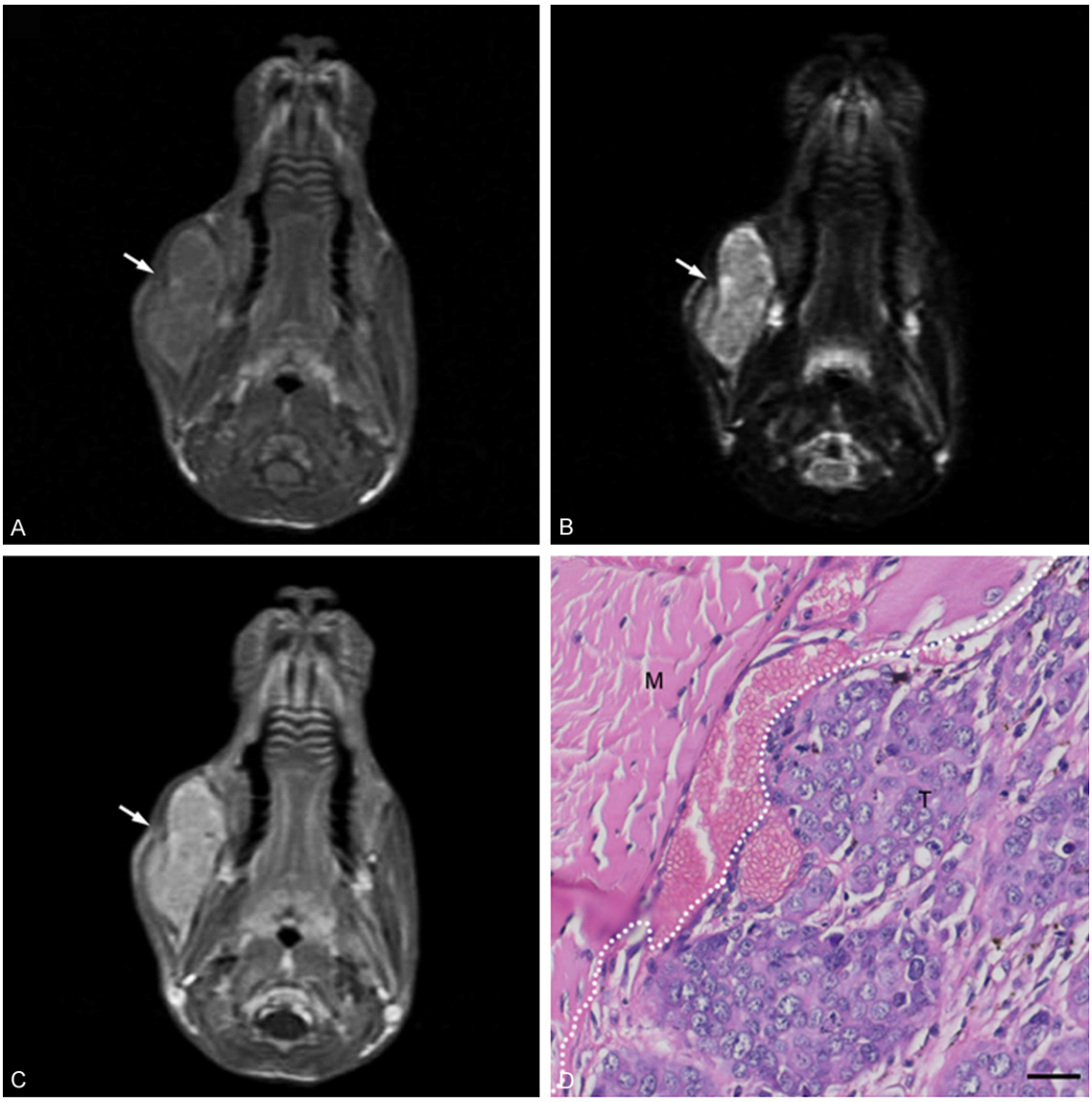

Figure 3. Representative magnetic resonance (MR) images of tumor (A-C) and hematoxylin-eosin (HE) staining section (D). (A) Dorsal T1-weighted image (T1WI) image. (B) Dorsal T2WI image. (C) Dorsal contrast-enhanced T1WI image. The white arrow in (A-C) shows the tumor. The dashed line in (D) shows the tumor border zone. The T and M represent the tumor and masseter muscle, respectively. The scale bar in (D) = 20 μm.

NY, USA), and all tissue images analyses were conducted with one experienced laboratory investigator and one board certificated pathologist.

For the HE section of each rabbit's tumor sample, the morphological and cellular analysis were undertaken to ascertain the presence of tumor and serve as guidance for the subsequent analysis. For quantitative hypoxic area analysis of PIMO staining sections, images without obvious and large necrosis were selected. The hypoxic areas were expressed as the PIMO area fraction (%), which was counted by calculating the percent of positive PIMO tumor area relative to the total tumor area (fPIMO, %) [21-26]. The VEGF IHC sections analyses were performed using quantitative scoring methods, including multiplying the percentage of immuno-positive cells by immune-positive intensity, which was similar to our previous method [19].

Statistical analysis

Spearman's rank correlation analyses were carried out between MER or SLE and the PIMO

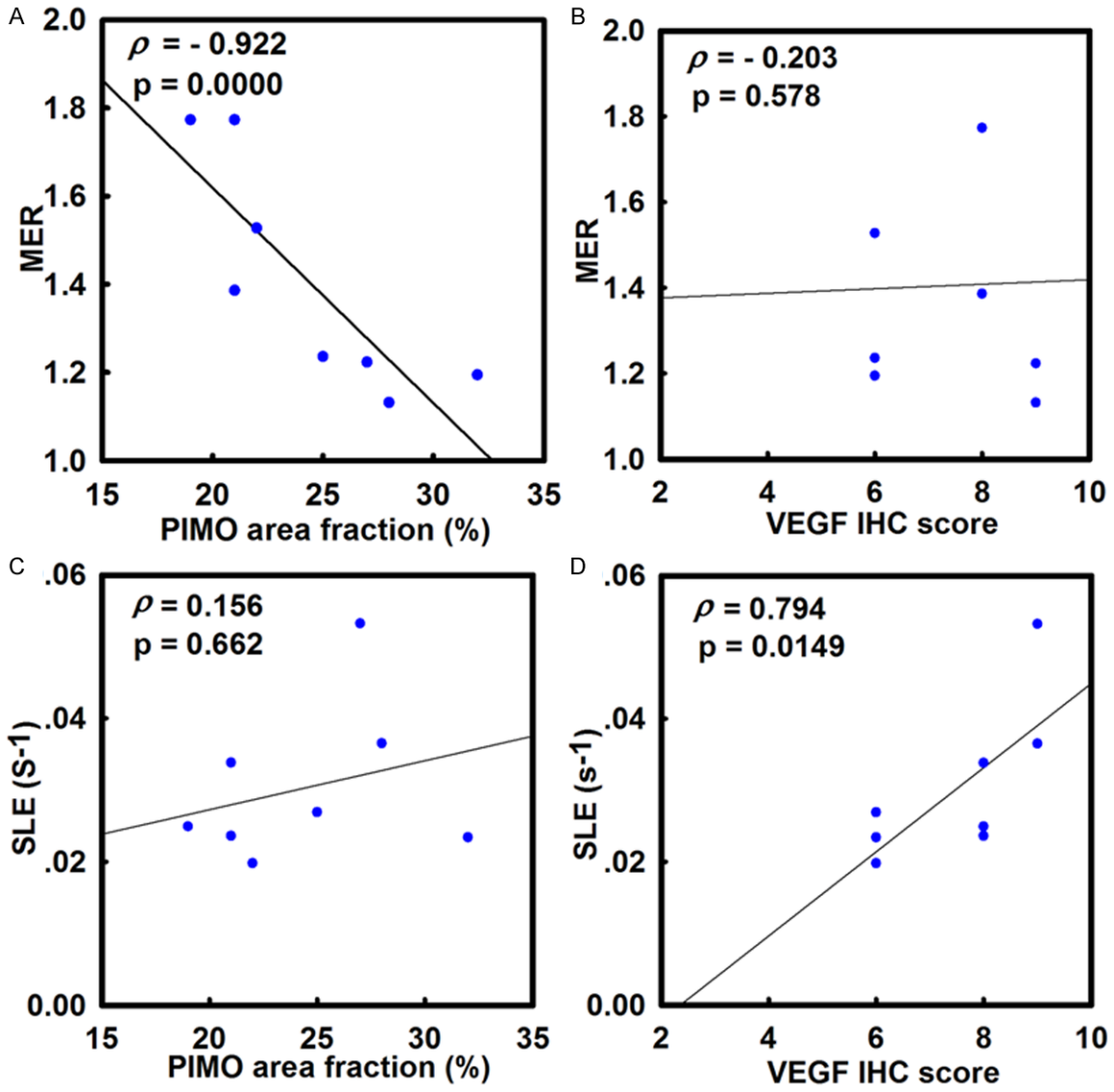

Figure 4. Correlation analysis of MER and SLE with the pathological staining results, respectively. A. Correlation between the MER and PIMO area fraction. B. Correlation between the MER and VEGF immunohistochemistry (IHC) score. C. Correlation between the SLE and PIMO area fraction. D. Correlation between the SLE and VEGF IHC score.

area fraction or the VEGF IHC score, respectively. Spearman's rank correlation coefficients were calculated by using SPSS 20.0 software (SPSS Inc., Chicago, IL, USA). The statistical significance level was set at α=0.05.

Results

Establishment and validation of the maxillofacial VX2 tumor model

VX2 tumors were successfully grown in eight of the eight rabbits' masseter muscles where they were inoculated. The tumor implantation rate was 100% and tumors were detectable at ten days post-inoculation by MRI (**Table 2**, **Figure 3**). During the observation period (approximately four weeks) of VX2 tumor inoculation; none of the rabbits died and there were no clinical signs in any of the inoculated rabbits. The tumor size ranged from 0.8 to 5.4 cm^3 (2.4 ± 1.45 cm^3 = Mean ± standard deviation [SD]; **Table 2**), which grew for ten to 24 days after implantation (**Table 2**). Lymph node metastases were detected in four implanted rabbits (4/8), and there were one to two metastatic lymph nodes (**Table 2**). Adjacent mandible tumor infiltration was found in one rabbit (1/8). The VX2 tumors were easily detected as masses inside the masseter

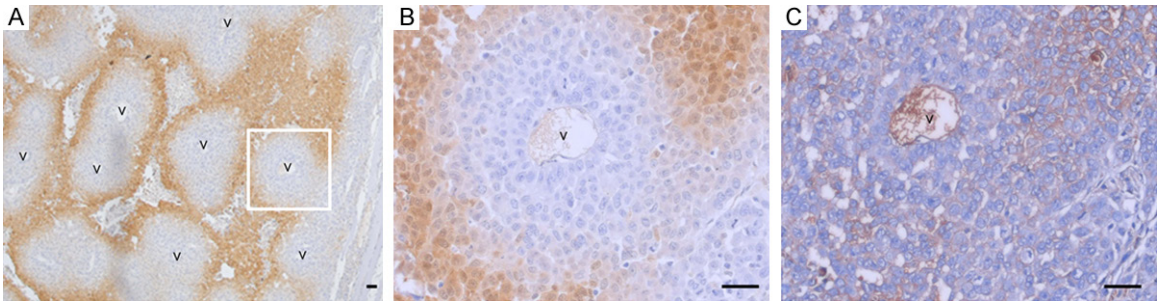

Figure 5. Representative histopathological slides of PIMO staining (A, B) and the serial slides of VEGF immunohistochemistry (IHC) staining (C). (A) PIMO staining. (B) The magnification image of PIMO staining for the white box inset of (A). (C) VEGF IHC staining for a section that is serial to the one with PIMO staining in (B). v in panels (A-C) represents the tumor vessel. The scale bar in (A-C) = 20 μm.

muscle by MRI examinations. The tumor masses showed iso-intensity (6/8, **Figure 3A**) or mixed hypo- and iso-intensity (2/8) in T1WI; mild hyper-intensity (4/8, **Figure 3B**) or iso-to-hyper-intensity (2/8) or mild hyper-intensity with central hyper-intensity(2/8) in T2WI; and homogeneous enhancement (5/8, **Figure 3C**) or heterogeneous enhancement (1/8) or heterogeneous enhancement with irregular central necrosis (2/8) in T1 contrast-enhanced images (**Table 2**). At necropsy, tumors in all eight rabbits were ascertained on gross pathological examination (data not shown) and HE staining (**Figure 3D**). Histologically, HE staining slides of all tumors showed neoplasms with typical VX2 tumor morphological characteristics located within the masseter muscle, which were accompanied with infiltration into the masseter muscle without a clear capsule (**Figure 3D**).

Semi-quantitative parameters of DCE-MRI

The MER and SLE measurements of tumors in eight rabbits are shown in **Table 2**, **Figure 4**. The MER value of eight VX2 tumors ranged from 1.132 to 1.773 (1.406 ± 0.258 [Mean ± SD]). These values had a significant negative correlation with the corresponding PIMO area fraction (ρ = -0.992, p = 0.0000002; **Figure 4A**), but there was no statistically significant correlation with the matched VEGF IHC score (ρ = -0.203, p = 0.578; **Figure 4B**). The SLE values of the eight VX2 tumors ranged from 0.0198 to 0.0532 s^{-1} (0.030 ± 0.011 s^{-1}). Correlation analysis showed that there was a statistically significant positive correlation between the SLE and corresponding VEGF IHC score (ρ = 0.794, p= 0.0149; **Figure 4D**). However, no statistically significant correlations were found between the SLE and matched PIMO area fraction (ρ = 0.156, p = 0.662; **Figure 4C**).

PIMO staining and VEGF IHC findings

PIMO staining for detecting tumor hypoxia was observed in the eight VX2 tumors of eight rabbit. The tumor hypoxic cells and areas stained by PIMO are shown in **Figure 5A** and **5B**. PIMO adducts were viewed predominantly at areas where they had some distance from the tumor blood vessel. Moreover, the further they are from the tumor blood vessel, the more intense the PIMO staining of the cells (**Figure 5A** and **5B**). The contiguous VEGF IHC staining section is shown in **Figure 5C**. The VEGF positive staining distribution overlapped the PIMO staining area with the exception that there is positive staining of cells adjacent to the tumor blood vessel (**Figure 5C**). No significant staining of negative control samples was observed (data not shown).

Discussion

In the current study, our results show that semi-quantitative DCE-MRI parameters can be used to predict tumor hypoxia in a maxillofacial VX2 rabbit model. We successfully validated the feasibility of DCE-MRI studies in this rabbit model. In addition, we have shown that the semi-quantitative method parameters can evaluate the state of oxygenation in tumors.

Oxygen is a critical factor of tumor progression. For a tumor size beyond 2 mm^3, its proliferation, growth and metastasis depend on the angiogenesis and lymphangiogenesis that sup-

ply adequate nutrients, oxygen and metabolites. When tumor cell expansion accelerates and exceeds the maximal effective diffuse distance of oxygen (100-150 μm) from the existing vascular supply and these subpopulations of tumor cells become hypoxic with a reduction in the normal level of tissue oxygen tension [27, 28], which is an important feature of numerous solid tumors [24, 29]. Mounting evidence suggests that hypoxia can induce increasing VEGF expression via a series of complicated mechanisms that include hypoxia-inducible factor 1 alpha (HIF-1α)-dependent or -independent mediated mechanisms [3, 8, 24, 27, 30]. Furthermore, hypoxia in tumors increases metastasis and resistance to chemotherapy and radiotherapy, resulting in poor prognosis and survival [27, 29, 30]. However, these pathophysiological changes cannot currently be detected except with biopsy and surgery; therefore, exploring surrogate molecular biomarkers *in vivo* are important to improving cancer treatment as noted above. In this study, our pathological results with PIMO staining and VEGF IHC showed that there is hypoxia and VEGF overexpression in VX2 tumors, which is in accordance with the previous studies [19, 30]. These results suggested that this VX2 tumor could be used as a reliable model to investigate tumor hypoxia.

Functional MRI has shown potential as a robust, noninvasive modality for imaging tumor hypoxia and includes blood oxygen level-dependent magnetic resonance imaging (BOLD-MRI) and DCE-MRI. Recently, some studies showed that BOLD-MRI can be used to monitor visceral adipose tissue oxygenation in humans [31], assess acute hypoxia in a C3H mammary carcinoma mice model [32] and depict hypoxia in breast invasive ductal carcinoma [33]. However, BOLD MRI depends on changes in paramagnetic deoxyhemoglobin within red blood cells, which is sensitive to oxygen in tumor perfusion. Actually, BOLD signals were used as a marker of acute hypoxia (perfusion-limited hypoxia), which was completely different from chronic hypoxia (diffusion-limited hypoxia) in many malignant tumors [3, 18, 24, 27, 32]. Therefore, BOLD-MRI was not a suitable modality for identifying tumor hypoxia due to diffusion-limited hypoxia.

DCE-MRI can be used to acquire a series of sequential images after fast bolus injection of contrast media combined with rapid acquisition methods [12, 34-37]. The acquisition process reflects the passage of a contrast agent through a particular tissue of interest. Therefore, dynamic images with variable enhancement over time were obtained, which could be used for drawing a time–intensity curve. These DCE-MRI data indirectly reflected the tumor microenvironment variables [14]. The time-intensity curve allows the direct measurement of some semi-quantitative parameters such as the MER, SLE, time to peak enhancement (TTP) and maximum absolute enhancement (SI_{max}) in a straightforward and simple way [16, 37]. MER represents a measurement of the degree of enhancement [16, 37]. Many studies have demonstrated that the enhancement was related to the vascular density within tissue, capillary permeability to contrast media, volume of the extracellular leakage space, angiogenic factors like VEGF, native T1-relaxation time of the tissue, and more, especially vascular density within the tissue and capillary permeability to contrast media [14, 34-37]. The oxygenation status within the tumor was also related to these factors [37]. In this study, we found that MER was negatively correlated with the identified hypoxia gradient and validated by PIMO staining, which could be explained by the aforementioned pathological base. Additionally, in a study of cervical cancer, the results showed that MER was correlated with the Eppendorf oxygen electrode measurements, which is considered as the reference standard for evaluating the tumor oxygen levels [38]. Combining this and our result suggests that MER can serve as a surrogate for tumor hypoxia measurements. SLE reflects the rate of enhancement [16, 35, 37]. SLE was mainly related to the vessel permeability [12, 35] and equal to the exchange rate constant K_{ep} (also called K_{21}), which was measured using quantitative pharmacokinetic models for DCE-MRI analysis [35]. VEGF, a potent vascular permeability and angiogenic factor, has been independently identified as a powerful molecule for tumor vascular hyperpermeability [37]. In this study, SLE was positively correlated with the overexpression of VEGF. This was consistent with Knopp et al's results that K_{21} was closely correlated with the tissue VEGF expression in breast tumors using pharmacokinetic parameter analysis [39]. Therefore, SLE can serve as a noninvasive biomarker for predicting tumor hypoxia.

There are several limitations in this study. First, quantitative pharmacokinetic analysis of the data from the present study was not performed. Quantitative indexes, including K^{trans}, K_{ep} and V_e, were not used in this study. Whether these indexes would provide more and stronger tumor functional information than the semi-quantitative parameters was not clearly determined. It is worth performing combined semi-and quantitative DCE-MRI research in the future. Second, we did not undertake intervention studies under hypoxia with radiotherapy or using vascular disrupting agents [40]. In the present proof-of-concept pilot study, we aimed to validate the feasibility of DCE-MRI for predicting *in vivo* hypoxia in a rabbit model. Further supplemental studies that employ radiotherapy using the same model will provide stronger evidence of its potential application and warrant and accelerate the clinical translation of these methods. Third, this study was undertaken in a VX2 tumor model, the rabbit tumor model. While it has histologic similarity to certain malignancies, it cannot mimic all the mammalian malignancies. The cell morphology and component differences in different tumors may have an effect on these parameters. Series studies using cancer and sarcoma models should be conducted to answer this question. Fourth, we investigated a range of tumors with different diameters; further studies with the same tumor diameters should be performed to validate whether there are significant variations in tumors with the same size.

In summary, the semi-quantitative parameters of DCE-MRI, MER and SLE, allow reliable evaluation of the tumor hypoxia in a maxillofacial VX2 rabbit model. This preclinical feasibility study shows that DCE-MRI could serve as a potentially non-invasive and translational tool for tumor pathophysiological feature evaluation in clinical practice.

Acknowledgements

The authors wish to thank Yunsheng Hu for MRI support; staff of animal research platform, Shanghai First People's Hospital, Shanghai Jiao Tong University for animal experiments support; and Shanghai First People's Hospital, Shanghai Jiao Tong University for "the best youth medical scholars" support. This research is financially supported by the National Natural Science Foundation of China (81271384, 81202133 and 81371623), the Natural Science Foundation of Shanghai Science and Technology Commission (No. 12ZR1424900), the State Scholarship Fund by China Scholarship Council for Dr. Linfeng Zheng.

Disclosure of conflict of interest

None.

Address correspondence to: Guixiang Zhang, Department of Radiology, Shanghai First People's Hospital, Shanghai Jiao Tong University, 100 Haining Road, No.3 Building, 117 Room, Shanghai 200080, China. Tel: +86-21-63240090-4166; Fax: +86-21-63240825; E-mail: guixiangzhang@sina.com; Zhuoli Zhang, Department of Radiology, Feinberg School of Medicine, Northwestern University, 737 North Michigan Avenue, Suite 1600, Chicago 60611, IL, USA. Tel: +1-312-695-5753; Fax: +1-312-926-5991; E-mail: zhuoli-zhang@northwestern.edu

References

[1] Helmlinger G, Yuan F, Dellian M and Jain RK. Interstitial pH and pO2 gradients in solid tumors in vivo: high-resolution measurements reveal a lack of correlation. Nat Med 1997; 3: 177-182.

[2] Jain RK and Forbes NS. Can engineered bacteria help control cancer? Proc Natl Acad Sci U S A 2001; 98: 14748-14750.

[3] Padhani AR, Krohn KA, Lewis JS and Alber M. Imaging oxygenation of human tumours. Eur Radiol 2007; 17: 861-872.

[4] Quail DF and Joyce JA. Microenvironmental regulation of tumor progression and metastasis. Nat Med 2013; 19: 1423-1437.

[5] Zhang X, Fryknas M, Hernlund E, Fayad W, De Milito A, Olofsson MH, Gogvadze V, Dang L, Pahlman S, Schughart LA, Rickardson L, D'Arcy P, Gullbo J, Nygren P, Larsson R and Linder S. Induction of mitochondrial dysfunction as a strategy for targeting tumour cells in metabolically compromised microenvironments. Nat Commun 2014; 5: 3295.

[6] Penet MF, Krishnamachary B, Chen Z, Jin J and Bhujwalla ZM. Molecular imaging of the tumor microenvironment for precision medicine and theranostics. Adv Cancer Res 2014; 124: 235-256.

[7] Lyng H, Sundfor K and Rofstad EK. Oxygen tension in human tumours measured with polarographic needle electrodes and its relationship to vascular density, necrosis and hypoxia. Radiother Oncol 1997; 44: 163-169.

[8] Evans SM and Koch CJ. Prognostic significance of tumor oxygenation in humans. Cancer Lett 2003; 195: 1-16.

[9] Krause BJ, Beck R, Souvatzoglou M and Piert M. PET and PET/CT studies of tumor tissue oxygenation. Q J Nucl Med Mol Imaging 2006; 50: 28-43.

[10] Braunagel M, Radler E, Ingrisch M, Staehler M, Schmid-Tannwald C, Rist C, Nikolaou K, Reiser MF and Notohamiprodjo M. Dynamic contrast-enhanced magnetic resonance imaging measurements in renal cell carcinoma: effect of region of interest size and positioning on interobserver and intraobserver variability. Invest Radiol 2015; 50: 57-66.

[11] Kim JY, Kim SH, Kim YJ, Kang BJ, An YY, Lee AW, Song BJ, Park YS and Lee HB. Enhancement parameters on dynamic contrast enhanced breast MRI : do they correlate with prognostic factors and subtypes of breast cancers? Magn Reson Imaging 2015; 33: 72-80.

[12] Zheng L, Sun P, Zheng S, Han Y and Zhang G. Functional dynamic contrast-enhanced magnetic resonance imaging in an animal model of brain metastases: a pilot study. PLoS One 2014; 9: e109308.

[13] Pickles MD, Manton DJ, Lowry M and Turnbull LW. Prognostic value of pre-treatment DCE-MRI parameters in predicting disease free and overall survival for breast cancer patients undergoing neoadjuvant chemotherapy. Eur J Radiol 2009; 71: 498-505.

[14] Martincich L, Montemurro F, De Rosa G, Marra V, Ponzone R, Cirillo S, Gatti M, Biglia N, Sarotto I, Sismondi P, Regge D and Aglietta M. Monitoring response to primary chemotherapy in breast cancer using dynamic contrast-enhanced magnetic resonance imaging. Breast Cancer Res Treat 2004; 83: 67-76.

[15] Meng Y, Zhang F, Blair T, Gu H, Feng H, Wang J, Yuan C, Zhang Z, Qiu B and Yang X. MRI of auto-transplantation of bone marrow-derived stem-progenitor cells for potential repair of injured arteries. PLoS One 2012; 7: e31137.

[16] Tang Y, Bernardin L, Booth TC, Miquel ME, Dilks P, Sahdev A and Rockall AG. Use of an internal reference in semi-quantitative dynamic contrast enhanced MRI (DCE MRI) of indeterminate adnexal masses. Br J Radiol 2014; 20130730.

[17] Zhang Z, Li W, Procissi D, Li K, Sheu AY, Gordon AC, Guo Y, Khazaie K, Huan Y, Han G and Larson AC. Antigen-loaded dendritic cell migration: MR imaging in a pancreatic carcinoma model. Radiology 2014; 132172.

[18] Gonzalez Hernando C, Esteban L, Canas T, Van den Brule E and Pastrana M. The role of magnetic resonance imaging in oncology. Clin Transl Oncol 2010; 12: 606-613.

[19] Zheng LF, Li YJ, Wang H, Zhao JL, Wang XF, Hu YS and Zhang GX. Combination of vascular endothelial growth factor antisense oligonucleotide therapy and radiotherapy increases the curative effects against maxillofacial VX2 tumors in rabbits. Eur J Radiol 2011; 78: 272-276.

[20] Yu YL, Lee MS, Juan CJ and Hueng DY. Calculating the tumor volume of acoustic neuromas: comparison of ABC/2 formula with planimetry method. Clin Neurol Neurosurg 2013; 115: 1371-1374.

[21] Raleigh JA, Chou SC, Tables L, Suchindran S, Varia MA and Horsman MR. Relationship of hypoxia to metallothionein expression in murine tumors. Int J Radiat Oncol Biol Phys 1998; 42: 727-730.

[22] Kennedy AS, Raleigh JA, Perez GM, Calkins DP, Thrall DE, Novotny DB and Varia MA. Proliferation and hypoxia in human squamous cell carcinoma of the cervix: first report of combined immunohistochemical assays. Int J Radiat Oncol Biol Phys 1997; 37: 897-905.

[23] Varia MA, Calkins-Adams DP, Rinker LH, Kennedy AS, Novotny DB, Fowler WC Jr and Raleigh JA. Pimonidazole: a novel hypoxia marker for complementary study of tumor hypoxia and cell proliferation in cervical carcinoma. Gynecol Oncol 1998; 71: 270-277.

[24] Rademakers SE, Lok J, van der Kogel AJ, Bussink J and Kaanders JH. Metabolic markers in relation to hypoxia; staining patterns and colocalization of pimonidazole, HIF-1alpha, CAIX, LDH-5, GLUT-1, MCT1 and MCT4. BMC Cancer 2011; 11: 167.

[25] Haustermans K, Hofland I, Van de Pavert L, Geboes K, Varia M, Raleigh J and Begg AC. Diffusion limited hypoxia estimated by vascular image analysis: comparison with pimonidazole staining in human tumors. Radiother Oncol 2000; 55: 325-333.

[26] Kaanders JH, Wijffels KI, Marres HA, Ljungkvist AS, Pop LA, van den Hoogen FJ, de Wilde PC, Bussink J, Raleigh JA and van der Kogel AJ. Pimonidazole binding and tumor vascularity predict for treatment outcome in head and neck cancer. Cancer Res 2002; 62: 7066-7074.

[27] Harris AL. Hypoxia--a key regulatory factor in tumour growth. Nat Rev Cancer 2002; 2: 38-47.

[28] Nishida N, Yano H, Nishida T, Kamura T and Kojiro M. Angiogenesis in cancer. Vasc Health Risk Manag 2006; 2: 213-219.

[29] Kyle AH, Baker JH and Minchinton AI. Targeting quiescent tumor cells via oxygen and IGF-I supplementation. Cancer Res 2012; 72: 801-809.

[30] Morfoisse F, Kuchnio A, Frainay C, Gomez-Brouchet A, Delisle MB, Marzi S, Helfer AC, Hantelys F, Pujol F, Guillermet-Guibert J, Bousquet C, Dewerchin M, Pyronnet S, Prats AC, Carmeliet P and Garmy-Susini B. Hypoxia

induces VEGF-C expression in metastatic tumor cells via a HIF-1alpha-independent translation-mediated mechanism. Cell Rep 2014; 6: 155-167.

[31] Zhou X, Yuan F, Ji WJ, Guo ZZ, Zhang L, Lu RY, Liu X, Liu HM, Zhang WC, Jiang TM, Zhang Z and Li YM. High-salt intake induced visceral adipose tissue hypoxia and its association with circulating monocyte subsets in humans. Obesity 2014; 22: 1470-1476.

[32] Nielsen T, Nielsen NC, Holm TH, Ostergaard L, Horsman MR and Busk M. Ultra-high field ^{1}H magnetic resonance imaging approaches for acute hypoxia. Acta Oncol 2013; 52: 1287-1292.

[33] Liu M, Guo X, Wang S, Jin M, Wang Y, Li J and Liu J. BOLD-MRI of breast invasive ductal carcinoma: correlation of R2* value and the expression of HIF-1alpha. Eur Radiol 2013; 23: 3221-3227.

[34] Harry VN, Semple SI, Parkin DE and Gilbert FJ. Use of new imaging techniques to predict tumour response to therapy. Lancet Oncol 2010; 11: 92-102.

[35] Padhani AR and Husband JE. Dynamic contrast-enhanced MRI studies in oncology with an emphasis on quantification, validation and human studies. Clin Radiol 2001; 56: 607-620.

[36] Shah GV, Fischbein NJ, Gandhi D and Mukherji SK. Dynamic contrast-enhanced MR imaging. Top Magn Reson Imaging 2004; 15: 71-77.

[37] Zahra MA, Hollingsworth KG, Sala E, Lomas DJ and Tan LT. Dynamic contrast-enhanced MRI as a predictor of tumour response to radiotherapy. Lancet Oncol 2007; 8: 63-74.

[38] Loncaster JA, Carrington BM, Sykes JR, Jones AP, Todd SM, Cooper R, Buckley DL, Davidson SE, Logue JP, Hunter RD and West CM. Prediction of radiotherapy outcome using dynamic contrast enhanced MRI of carcinoma of the cervix. Int J Radiat Oncol Biol Phys 2002; 54: 759-767.

[39] Knopp MV, Weiss E, Sinn HP, Mattern J, Junkermann H, Radeleff J, Magener A, Brix G, Delorme S, Zuna I and van Kaick G. Pathophysiologic basis of contrast enhancement in breast tumors. J Magn Reson Imaging 1999; 10: 260-266.

[40] Tozer GM, Kanthou C and Baguley BC. Disrupting tumour blood vessels. Nat Rev Cancer 2005; 5: 423-435.